Available online at www.sciencedirect.com
SCIENCE DIRECT®
Journal of Molecular Spectroscopy 221 (2003) 116–120
Journal of MOLECULAR SPECTROSCOPY
www.elsevier.com/locate/jms

The dipole moment of HOCl in $v_{OH} = 4$

Andrea Callegari,[a] Patrice Theulé,[a] Roman Schmied,[a,1] Thomas R. Rizzo,[a] and J.S. Muenter[b,*]

[a] *Laboratoire de chimie physique moléculaire (LCPM), Ecole Polytechnique Fédérale de Lausanne, Lausanne 1015, Switzerland*
[b] *Department of Chemistry, University of Rochester, Rochester, NY 14627, USA*

Received 23 April 2003; in revised form 14 May 2003

Abstract

Pulsed laser excitation and photofragment detection methods are used to observe the $17_{0,17} \leftarrow 16_{1,16}$ pure rotational transition within the $v_{OH} = 4$ vibrational state of $HO^{35}Cl$. Microwave frequency and Stark effect measurements give $v_0 = 27484.33(10)$ MHz and $\mu_b = 1.562(9)$ D. The dependence of μ_b, which is approximately parallel to the OH bond, on the level of OH stretch excitation appears linear and is consistent with that of H_2O over the same 0–14 000 cm^{-1} energy range.

Keywords: Dipole moment; Stark effect; Excited vibrational states; Double resonance; Pulsed laser; Photofragment detection; Hypochlorous acid

1. Introduction

Chemists have long used electric dipole moments as convenient and intuitive descriptions of electronic charge distributions in molecules [1–4]. Dipole moments also provide stringent tests of ab initio wavefunctions, since dipole moment calculations converge differently than those of energies, and variational methods that give comparable energies can produce quite different moments [5–7].

Dipole moments have been measured for a large number of molecules in their ground vibrational states, with the vast majority of these data obtained from observing the Stark effect in pure rotational spectra. Extending Stark effect measurements to high energy states accessed by vibration–rotation transitions has been difficult, because Doppler widths of infrared and visible transitions are typically larger than the majority of available Stark splittings [8–10]. We have recently developed a new approach to Stark effect measurement that uses pulsed laser excitation and spectroscopic detection of photofragments to observe either high-resolution microwave spectra or electric field induced quantum beats in highly excited vibrational states [11–13]. In our first experiment of this type, described in Paper I [11], we measured the Stark effect on a pure rotational transition in $HO^{35}Cl$ molecules containing two quanta of OH stretching excitation ($v_{OH} = 2$). The present report describes an extension of this work to HOCl with $v_{OH} = 4$, which lies about 14 000 cm^{-1} above the ground state. Combined with information on HOCl dipole moments in $v_{OH} = 0$ and 2, these new measurements allow us to observe the evolution of the dipole moment over a wide range of vibrational energy, and provide stringent tests of calculated dipole surfaces.

2. Experimental approach

The photodissociation-detected microwave spectroscopy approach used in these measurements is an offshoot of the double resonance overtone photofragment spectroscopy techniques that we have developed to measure the unimolecular dissociation dynamics of a number of small molecules [14–20]. In those experiments, we use an infrared laser pulse to excite either the fundamental or a low overtone transition of the OH

* Corresponding author. Fax: 1-585-473-6889.
E-mail address: muenter@chem.rochester.edu (J.S. Muenter).
[1] Present address: Department of Chemistry, Princeton University, Princeton, NJ 08544, USA.

0022-2852/$ - see front matter © 2003 Elsevier Science (USA). All rights reserved.
doi:10.1016/S0022-2852(03)00173-5

stretch, pre-selecting reactant molecules in single rotational states. A second laser pulse promotes only the molecules in this intermediate level to a high rovibrational level on the ground electronic state that is above the threshold to produce OH dissociation fragments. A third laser then probes the OH fragments via LIF in the A–X band. This approach permitted us to obtain photofragment excitation spectra of resonance states embedded in the dissociation continuum as well as to monitor the dissociation dynamics from these individual rovibrational states. In the case of HOCl, we have used both the $(200) \leftarrow (000)$ and $(400) \leftarrow (000)$ overtone bands of the OH stretch for the state-selection transition to reach dissociative states with $v_{OH} = 6$–8 [17–20].

The present experiment uses the $(400) \leftarrow (000)$ band for state selection and the $(600) \leftarrow (400)$ band for dissociation. Detuning the frequency of the second laser so that it is no longer resonant with the state populated by the first laser breaks the excitation chain, causing the OH LIF signal to disappear. If the second laser is tuned to excite HOCl from a (400) rotational level adjacent to the state populated by the first laser, as shown in the inset of Fig. 1, a pure rotational transition connecting the final state of the first laser absorption and the initial state of the second laser excitation reinstates the chain and enables dissociation. In this way we detect the occurrence of the microwave transition by the appearance of the OH LIF signal. Stark data for the microwave transition allow us to extract the dipole moment of the (400) state.

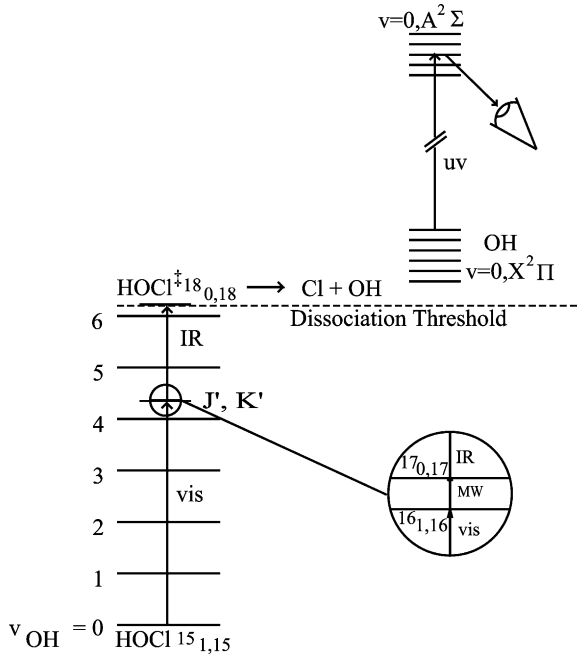

Fig. 1. Double resonance dissociation of HOCl: $v_{OH} = 0$, $J'', K'' \rightarrow v_{OH} = 4$, $J', K' \rightarrow v_{OH} = 6, J, K$. As shown in the inset, a microwave transition (the $17_{0,17} \leftarrow 16_{1,16}$ in this case) can be observed in triple resonance by slightly changing the second laser frequency. The excitation process, in either 2 or 3 steps, is detected by observing LIF from OH fragments generated by the photodissociation.

Following the procedure described by Sinha in his work [21] on this molecule, we produce HOCl by flowing a low pressure mixture of Cl_2 and H_2O through a column of glass beads packed with HgO. The HOCl generated in this fashion slowly flows through a gas cell at a total pressure of approximately 20 mTorr. As discussed in Paper I, the Stark field is generated by a set of parallel plate electrodes having a 1 cm spacing. Microwave radiation from a Hewlett–Packard 83751A synthesizer and a DBS 2640X218 frequency doubler enters the cell via semi-rigid coaxial cable, where it is coupled to the Stark electrodes using a K-band waveguide to coaxial converter. Infrared, visible, and ultraviolet laser pulses enter and exit the cell through baffled sidearms and are overlapped half way between the electrodes at a distance of 1 cm from their upper edges. An $f/1$ lens above the electrodes images the OH fluorescence through a filter and onto a photomultiplier tube. We control the laser pulse timing, microwave frequency, and data acquisition by CAMAC modules interfaced to a PC. We measure Stark voltages with a calibrated voltage divider and Hewlett–Packard 3456A voltmeter, and determine the electrode spacing with precision gauge blocks. The visible excitation pulse at about $13\,500\,cm^{-1}$ emanates from a Nd:YAG pumped dye laser operating on LDS751 laser dye. The infrared pulse at about $5700\,cm^{-1}$ that dissociates the HOCl molecules is obtained by mixing the output of a dye laser operating on DCM with the fundamental output of a single-mode Nd:YAG laser in lithium niobate.

The HOCl dissociation threshold is about $160\,cm^{-1}$ above the rotationless (600) level, so at least this much rotational energy is required to detect the microwave transition by observing OH dissociation fragments. This fact, together with the strongly prolate nature of HOCl, significantly limits the number of transitions available in the conventional microwave portion of the spectrum. Suitable transitions occur when the J state in the $K = 1$ manifold is nearly degenerate with the $J + 1$ state in the $K = 0$ manifold, and the most appropriate microwave transition that we can access in (400) is the $17_{0,17} \leftarrow 16_{1,16}$ at 27.5 GHz. As indicated in Fig. 1, the following excitation scheme was used to observe the $17_{0,17} \leftarrow 16_{1,16}$ microwave signal: (000), $15_{1,15} \rightarrow (400)$, $16_{1,16} \rightarrow (400)$, $17_{0,17} \rightarrow (600)$, $18_{0,18}$. The pure rotational transition occurs during the time-delay between the visible and the infrared laser pulses, and this limits the time available to generate the microwave signal. Longer delay times generate narrower microwave absorption lines until the pulse delay is comparable to the transit time of HOCl molecules across the laser beams, which then becomes the limiting measurement time. The optimum time-delay is 500 ns, which produces a minimum linewidth of 1.8 MHz FWHM. Fig. 2 plots the

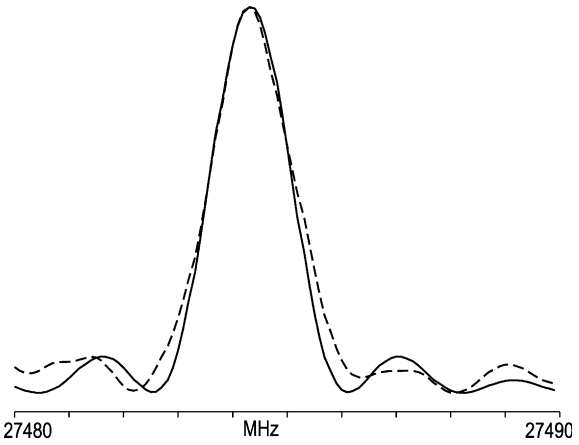

Fig. 2. The $17_{0,17} \leftarrow 16_{1,16}$ pure rotational transition in $v_{OH} = 4$ of $HO^{35}Cl$ in zero electric field. The solid curve is the Rabi, two-level lineshape for a 500 ns delay between the visible and infrared laser pulses, and has a FWHM of 1.8 MHz. The dashed curve is experimental data.

measured data for the $17_{0,17} \leftarrow 16_{1,16}$ transition in the absence of a Stark field (dashed line) together with a fit of the two level transition probability [22] for a 500 ns measurement time (solid line). The fit adjusts the transition frequency and normalizes the peak amplitude, yielding $v_0 = 27484.33(10)$ MHz.

This zero-field transition splits into 17 unresolved Stark components when the M degeneracy is lifted by the Stark field. Fortunately, we can model the lineshape with a precise dipole moment and an approximate value for the microwave E field. This is shown in Fig. 3, which displays data for 1400 V/cm as a dashed line, along with

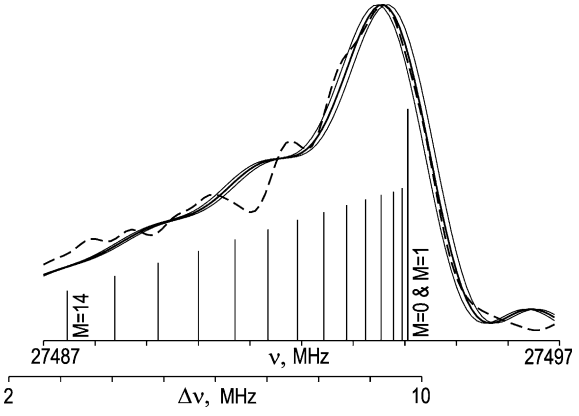

Fig. 3. The microwave transition shown in Fig. 2, in a 1400 V/cm Stark field. The dashed curve shows experimental data, while the three solid curves are calculated lineshapes. The heavy solid line has μ_b adjusted to 0.001 D larger than the optimal value, so the high frequency edge of the solid and dashed curves are resolved. The two lighter solid lines use dipole moments differing by ±0.5% from the optimum value. The frequency axes display absolute and relative positions of the Stark shifted signal. Note that the experimental data do not extend to low enough frequency to include the weakest two Stark components.

three different calculated wave forms. The high frequency edge of the signal accurately determines the dipole moment, as indicated by the three curves which differ only by varying the moment by ±0.5% from a near optimum value. The slow rise of the signal with increasing frequency is much less sensitive to the moment, but exhibits moderate dependence on the microwave E-field strength. As long as the high frequency portion of the signal is not saturated, the optimum dipole moment is independent of the microwave field used to calculate the lineshape. Being careful to avoid saturation, we recorded data of this type for Stark fields from 1000 to 2000 V/cm.

3. Analysis

The Stark effect for the $17_{0,17} \leftarrow 16_{1,16}$ transition is dominated by the dipole moment matrix element connecting the two rotational states involved in the transition. This matrix element, evaluated with Wang linear combinations of symmetric top wavefunctions, has the general form [23]

$$\mu_{J,K,M\to J-1,K+1,M} = \mu_b \sqrt{\frac{(J^2-M^2)(J-K)(J-K-1)}{2J^2(2J-1)(2J+1)}}, \tag{1}$$

with $J = 17$, $K = 0$. The second-order Stark effect associated with this matrix element is given by

$$\Delta v = \frac{\mu_b^2 E_{dc}^2}{h^2 v_0}\left(\frac{(J^2-M^2)(J-K)(J-K-1)}{J^2(2J-1)(2J+1)}\right), \tag{2}$$

where Δv is the Stark shift, μ_b is the dipole moment component along the b inertial axis, E_{dc} is the Stark field, and v_0 is the zero-field frequency. The frequency shift given by Eq. (2) accounts for more than 90% of the total observed Stark shift, making these experiments sensitive to only the b-component of the permanent dipole moment.

While Eq. (2) gives a good picture of the observed Stark effect, the data analysis uses a more complete expression that contains small contributions from additional μ_b matrix elements and fourth-order interactions from the matrix element in Eq. (1). We make some additional corrections that individually are small relative to the precision of the data, but taken together give a net contribution of about one standard deviation since they all increase the dipole moment. These include accounting for the asymmetry of the molecule, the slight lifting of the $M = \pm 1$ degeneracy by chlorine hyperfine structure [23] and the small decrease in the Stark field that the molecules experience from being close to the edge of the electrodes. This last correction was made using the SIMION program [24]. The a-component of the HOCl dipole moment does not make a significant contribution

Table 1
Stark fields, dipole moments fit to data, and calculated frequencies for the $M = 0$ components

E_{dc} (V/cm)	μ_b (D)	ν ($M = 0$) (MHz, calc.)
983.7	1.592(15)	27489.51
1180.2	1.555(10)	27491.44
1377.0	1.561(8)	27494.08
1475.4	1.562(7)	27495.54
1573.8	1.569(6)	27497.20
1672.2	1.562(5)	27498.73
1770.8	1.561(5)	27500.45
1869.0	1.563(4)	27502.34
1967.7	1.563(4)	27504.29

to this Stark effect because μ_a is relatively small (0.36 D in the ground state [25,26]) and the a-type terms all have large energy denominators. It is thus possible to calculate the Stark shift, $\Delta\nu$, for each M value in terms of a single parameter, μ_b. The frequencies of individual Stark components are shown in the stick diagram portion of Fig. 3. The dashed curve shows experimental data for 1400 V/cm, and the three solid curves are calculated signals, each using a slightly different dipole moment value. The calculated curves were generated from the accurate Stark shift expression, the two level Rabi lineshape [22] for each M component, and an approximate value for the microwave E field. The calculated signals are normalized to the peak intensity of the observed data. For the heavy solid line, the value of μ_b is 0.001 D larger than optimum so the two waveforms can be distinguished at the high frequency edge of the figure. The two lighter solid lines use dipole moments differing by $\pm 0.5\%$ from the optimum value. The frequency axes in Fig. 3 display absolute and relative positions of the Stark components.

For each electric field used, the calculated and observed signals were displayed together and μ_b was varied until the high frequency edge of the two waveforms were superimposed. The dipole moments obtained in this way are listed in Table 1, along with E_{dc} values and calculated frequencies for the $M = 0$ Stark component. The experimental accuracies listed with the dipole moments are based on maximum Stark shifts deviating from the calculated values by no more than 100 KHz. A weighted average of the individual dipole moment values listed in Table 1 gives $\mu_b = 1.562(9)$ D, where the uncertainty includes both statistical and calibration contributions.

4. Discussion

The dipole moment data that we have obtained for vibrationally excited states of $HO^{35}Cl$ are limited to μ_b components. While we have devoted substantial effort to both microwave double resonance and Stark induced quantum beat experiments that are sensitive to μ_a, the combination of spectroscopic and HOCl dissociation requirements has made it impossible to obtain μ_a values for vibrationally excited states. In the absence of μ_a, we use the geometry of HOCl and a bond moment model to interpret μ_b. The a inertial axis is just 2° from the O–Cl bond axis and this angle varies by only 0.2° for the excited states in question. Thus the O–Cl bond moment has a negligible projection on the b axis. The OH bond lies at a 15° angle relative to the b axis, making $\mu_b = \mu_{OH}\cos(15°) = 0.97\mu_{OH}$ [27]. Thus, to a quite good approximation, the μ_b values reported here represent OH bond moments.

As shown in Fig. 4, μ_b appears to vary linearly with vibrational energy. Such behavior is expected [28–31], even in the presence of mechanical ($\omega_e x_e$) and electrical ($d^2\mu/dR^2$) anharmonicities, if the energy is localized to the extent that the vibrational excitation can be treated like a single oscillator. The linear dipole moment behavior that we observe in HOCl is thus evidence for local mode [32,33] behavior—that is, that the OH stretching mode is not significantly mixed with other modes for energies up to $\approx 14\,000\ cm^{-1}$. This is consistent with our earlier observation of just small, local perturbations in $v_{OH} = 6$ rotational energy level structure [18].

The only other molecule for which dipole moments are available for excited OH stretching vibrations is water, and we have measured water moments for excited states containing 1, 4, 5, and 8 quanta of OH stretching vibration [12,13,34]. Even though water is known to be a good local mode molecule [32,33], vibrational excitation causes small changes in geometry and slight reorientations of inertial axes, and hence the dipole moment components projected on these axes change [13]. While

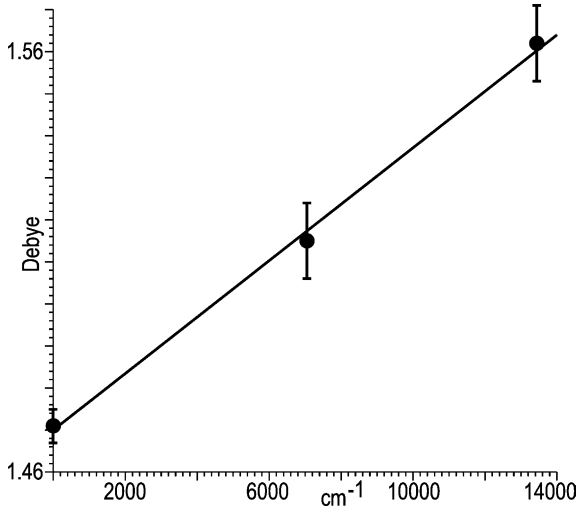

Fig. 4. Dipole moment data for $HO^{35}Cl$ plotted as a function of vibrational energy. The three moments plotted here are from comparably high J transitions and centrifugal distortion is not an issue in this comparison [11,26].

these effects make it difficult to obtain quantitative OH bond moments from μ_a and μ_b values for OH stretching states of H_2O, the data for $v_{OH} = 0$, 1, and 4 are consistent with our HOCl measurements. However, it is important to note that the systematic increase in the H_2O moments stops at $v_{OH} = 4$. The dipole moment of $v_{OH} = 5$ of H_2O is almost identical to that of $v_{OH} = 4$, and the moment slightly decreases for $v_{OH} = 8$. This change is necessary, since the dipole moment of very highly excited OH stretching states of water must approach the 1.655 D moment of OH [35]. It is not clear at what point the OH bond moment in HOCl will begin to decrease, but it must do so at sufficiently high excitation levels of excitation.

The changes in molecular charge distribution with high energy vibrational excitation are complicated, but certainly important to many fundamental chemical processes. While it is clear that dipole moment data alone cannot provide a complete understanding of these changes, we believe that these experiments are important steps toward a more detailed picture of high energy, reactive chemical species.

Acknowledgments

We gratefully acknowledge support by the Swiss National Science Foundation Grant Number 2000-5926.99 and by the European Union Training and Mobility Program, Project SPHERS, Contract Number HPRN-CT-2000-00022. We thank Prof. A. Bauder, ETHZ, for lending us his microwave frequency doubler.

References

[1] The Handbook of Chemistry and Physics, The Chemical Rubber Co., Cleveland, 2002, pp. 9-45–9-51.
[2] Landolt-Bornstein Numerical Data and Functional Relationships in Science and Technology, New Series, 11/6 (1974), 11/14a (1982), 11/14b (1983), 11/19c, Springer, Heidelberg, 1992.
[3] R.D. Nelson, D.R. Lide, A.A Maryott, Selected Values of Electric Dipole Moments for Molecules in the Gas Phase, Natl. Stand. Ref. Data Ser., US National Bureau of Standard, Washington, 1967.
[4] P. Debye (Ed.), The Dipole Moment and Chemical Structure, translated by W.M. Deans, Blackie & Sons Ltd., London, 1931.
[5] A. Halkier, W. Klopper, T. Helgaker, P. Jorgensen, J. Chem. Phys. 111 (1999) 4424–4430.
[6] G. de Oliveire, C.E. Dykstra, Theor. Chem. Acc. 11 (1999) 435–438.
[7] H.G. Kjaergaard, K.J. Bezar, K.A. Brooking, Mol. Phys. 96 (1999) 1125–1138.
[8] K. Nakawa, Y. Moriwaki, T. Shimizu, Opt. Lett. 14 (1989) 488–490.
[9] J.A. Dodd, A.M. Smith, W.A. Klemperer, J. Chem. Phys. 88 (1988) 15–19.
[10] P.H. Vaccaro, J.L. Kinsey, H.-L. Dai, R.W. Field, J. Chem. Phys. 78 (1983) 3659–3664.
[11] J.S. Muenter, J. Rebstein, A. Callegari, T.R. Rizzo, J. Chem. Phys. 111 (1999) 3488–3493.
[12] A. Callegari, P. Theule, J.S. Muenter, R.N. Tolchenov, N. Zobov, O. Polyanski, J. Tennyson, T.R. Rizzo, Science 297 (2002) 993–995.
[13] A. Callegari, P. Theule, J.S. Muenter, T.R. Rizzo, J. Chem. Phys. (to be published).
[14] B. Kuhn, T.R. Rizzo, J. Chem. Phys. 112 (2000) 7461–7474, and refs. therein.
[15] P.R. Fleming, M.Y. Li, T.R. Rizzo, J. Chem. Phys. 94 (1991) 2425–2437.
[16] F. Reiche, B. Abel, R.D. Beck, T.R. Rizzo, J. Chem. Phys. 112 (2000) 8885–8898;
J. Chem. Phys. 116 (2002) 10267–10276.
[17] M.R. Wedlock, R. Jost, T.R. Rizzo, J. Chem. Phys. 107 (1997) 10344–10347.
[18] A. Callegari, J. Rebstein, J.S. Muenter, R. Jost, T.R. Rizzo, J. Chem. Phys. 111 (1999) 123–133.
[19] A. Callegari, J. Rebstein, R. Jost, T.R. Rizzo, J. Chem. Phys. 111 (1999) 7359–7368.
[20] A. Callegari, R. Schmied, P. Theule, J. Rebstein, T.R. Rizzo, Phys. Chem. Chem. Phys. 3 (2001) 2245–2252.
[21] G. Dutton, R.J. Barnes, A. Sinha, J. Chem. Phys. 111 (1999) 4976–4992.
[22] N.F. Ramsey, in: Molecular Beams, Oxford University Press, New York, 1956, p. 119.
[23] C.H. Townes, A.L. Schawlow, Microwave Spectroscopy, McGraw-Hill, New York, 1955.
[24] D.A. Dahl, SIMION 3D Version 6.0, Idaho National Engineering Laboratory, MS 2208, P.O. Box 1625, Idaho Falls, ID 83415.
[25] G. Modugno, P. De Natale, M. Bellini, M. Inguscio, G. Di Lonardo, L. Fusina, J. Vander Auwera, J. Opt. Soc. Am. B 13 (1996) 1645–1649.
[26] H.E.G. Singbeil, W.D. Anderson, R.W. Davis, M.C.L. Gerry, E.A. Cohen, H.M. Pickett, F.J. Lovas, R.D. Suenram, J. Mol. Spectrosc. 103 (1984) 466–485.
[27] A.M. Mirri, F. Scappini, G. Cazzoli, J. Mol. Spectrosc. 38 (1971) 218–227.
[28] E.W. Kaiser, J. Chem. Phys. 53 (1970) 1686–1703.
[29] J.W. Raymonda, J.S. Muenter, W.A. Klemperer, J. Chem. Phys. 52 (1970) 3458–3461.
[30] D.K. Hinderman, C.D. Cornwall, J. Chem. Phys. 48 (1968) 4148–4154.
[31] S.A. Rice, W.A. Klemperer, J. Chem. Phys. 27 (1957) 573–579.
[32] M.S. Child, R.T. Lawton, Chem. Phys. Lett. 87 (1982) 217–220.
[33] M.S. Child, L. Halonen, Adv. Chem. Phys. 57 (1984) 1–58.
[34] S.L. Shostak, W.L. Ebenstein, J.S. Muenter, J. Chem. Phys. 94 (1991) 5875–5882.
[35] K.I. Peterson, G.T. Fraser, W.A. Klemperer, Can. J. Phys. 62 (1984) 1502–1507.